Electronic Supplementary Material (ESI) for Nanoscale Advances.

Supporting Information

Tunable physical properties in Bi-based layered supercell multiferroics embedded with Au nanoparticles

Jianan Shen, [a] Zihao He, [b] Di Zhang, [a] Ping Lu, [c] Zhongxia Shang, [a] Matias Kalaswad, [b] Haohan Wang, [d] Xiaoshan Xu, [d] and Haiyan Wang[ab]*

a School of Materials Engineering, Purdue University, West Lafayette, Indiana 47907, United States.

b School of Electrical and Computer Engineering, Purdue University, West Lafayette, Indiana 47907, United States.

c Sandia National Laboratory, Albuquerque, New Mexico 87185, United States.

d Department of Physics and Astronomy, University of Nebraska-Lincoln, Lincoln, Nebraska 68588, United States.

Section 1. Supplementary XRD results

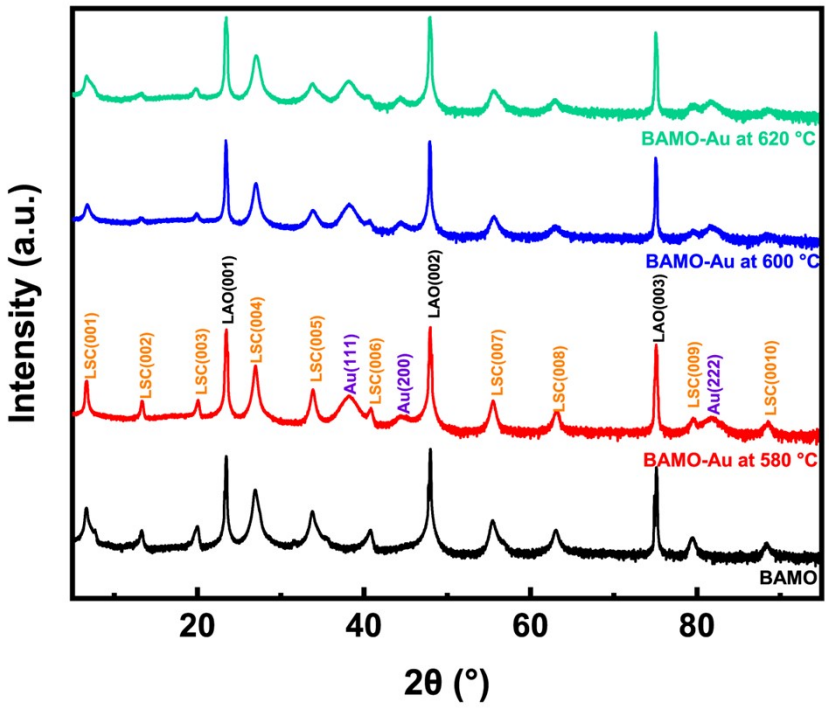

Figure S1. XRD θ-2θ diffraction results of BAMO and BAMO-Au epitaxial thin films on LAO(001) substrate at various growth temperatures.

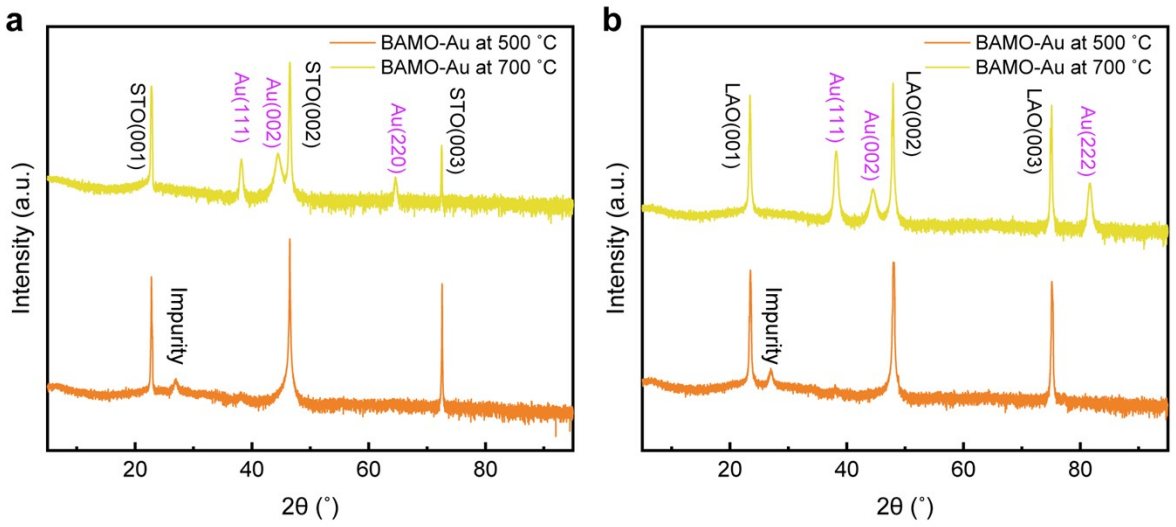

Figure S2. XRD θ-2θ diffraction results of BAMO-Au films grown at 500 C and 700℃ on (a) STO(001) substrate and (b) LAO(001) substrate. The results clearly show no LSC peaks at these two extreme temperatures.

Section 2. Plan-view STEM images

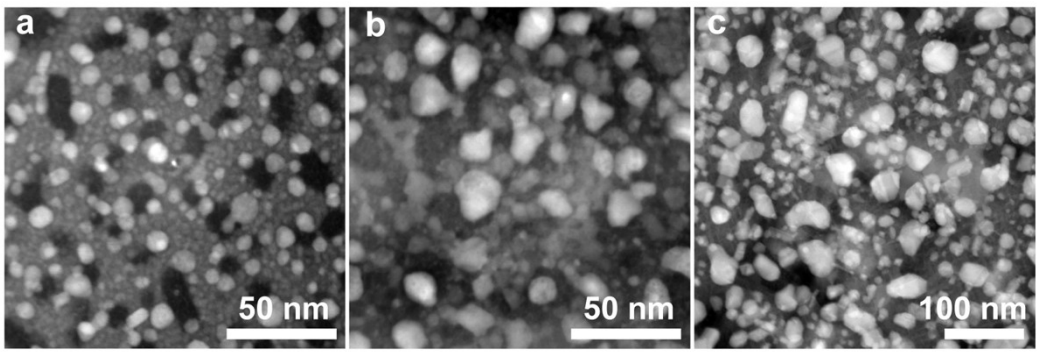

Figure S3. Plan-view STEM images of BAMO-Au thin films on STO substrate grown at (a) 580℃, (b) 600℃ and (c) 620℃, respectively, displaying significant variation in size of gold NPs.

Section 3. Transmittance measurement, bandgap calculation and plasmonic simulation.

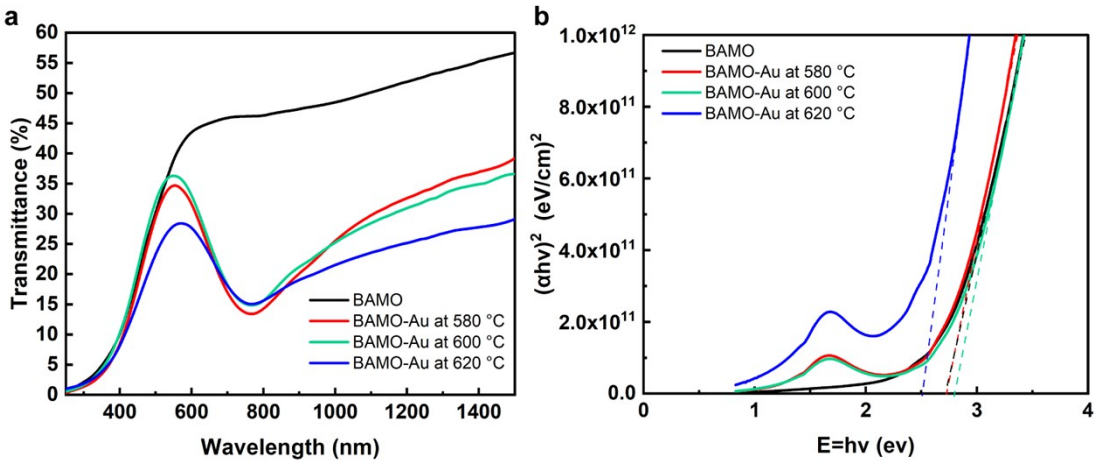

Figure S4. (a) Optical transmission spectra of BAMO-Au thin films on LAO (001) substrate, displaying a similar phenomenon of plasmonic absorption due to Au NPs. (b) Tauc plot is used to determine the bandgap of BAMO-Au thin films.

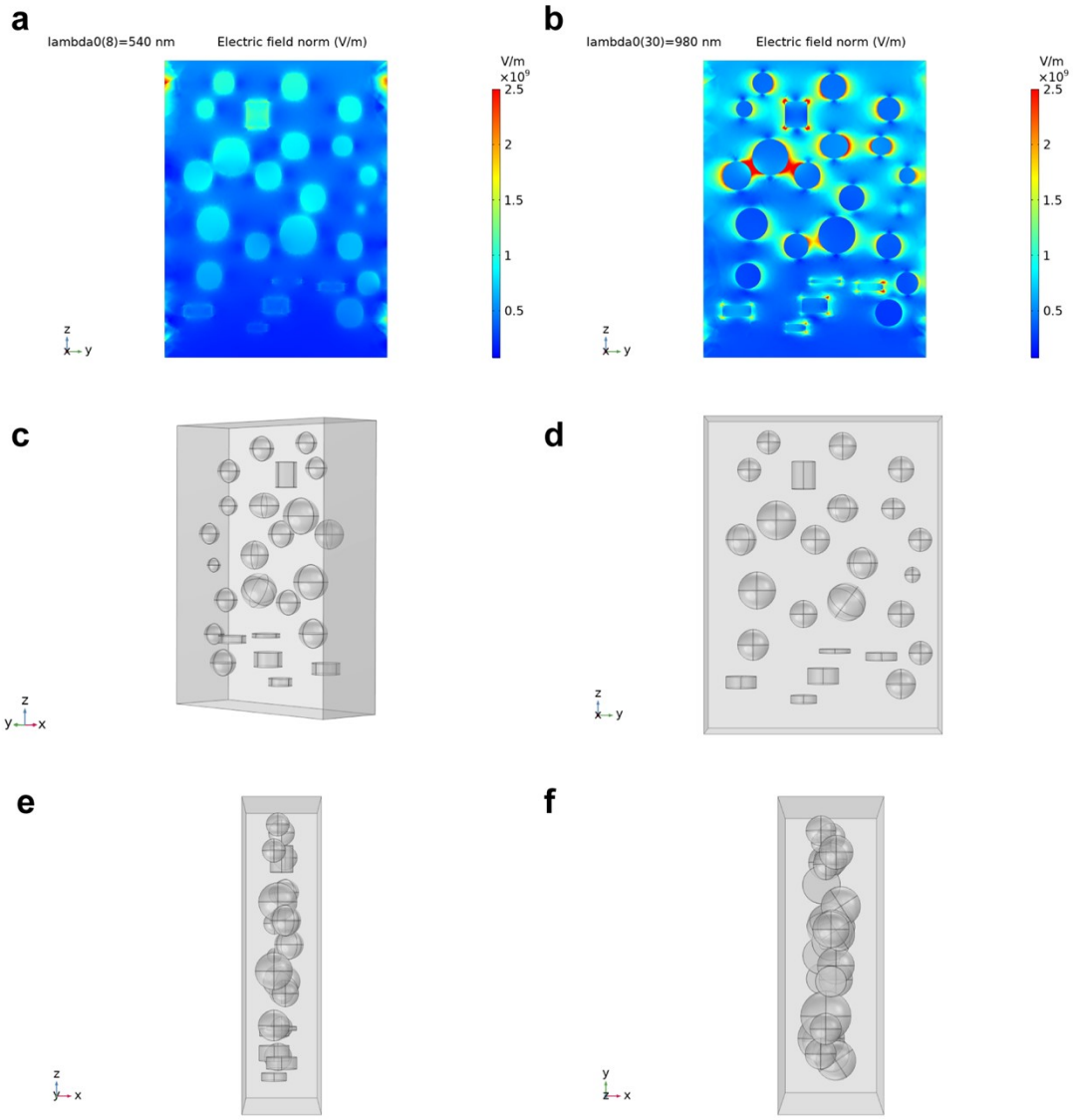

Figure S5. Simulation of plasmonic effect using COMSOL Multiphysics® version 5.6 software at (a) λ = 540 nm, (b) λ = 980 nm. (c) The 3D model set-up for simulation created by COMSOL software. (d)-(f) The side-view images projected from three axes.

Section 4. Variable angle spectroscopic ellipsometric data and imaginary part of permittivity

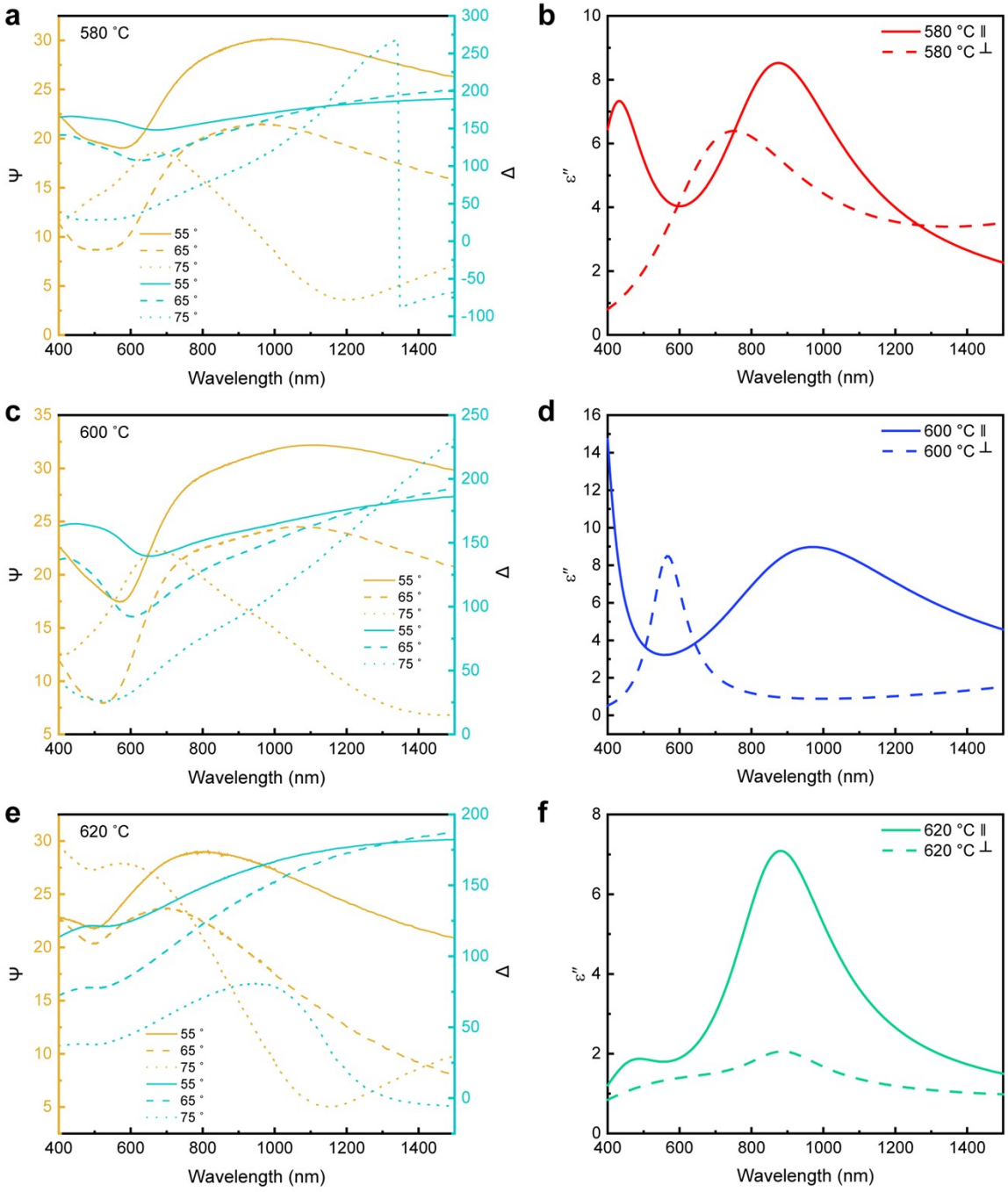

Figure S6. (a), (c), (e) are the experimental psi and delta data measured by ellipsometer for three deposition temperatures. (b), (d), (f) are the imaginary part of permittivity for films grown at three temperatures.

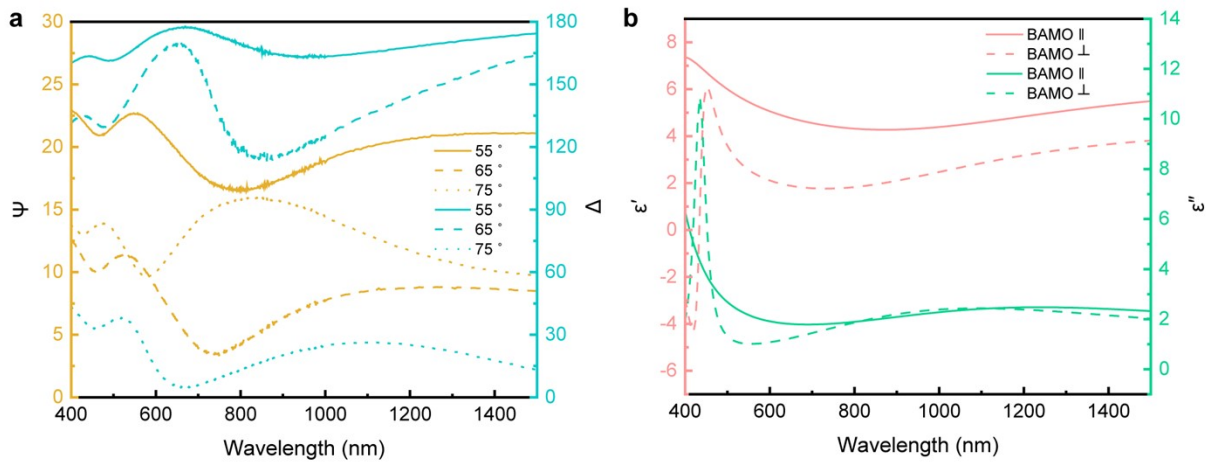

Figure S7. (a) The experimental psi and delta data measured by ellipsometer for BAMO films. (b) The real and imaginary part of permittivity along in-plane and out-of-plane directions for BAMO films.

Section 5. Ferromagnetic and ferroelctric characterization

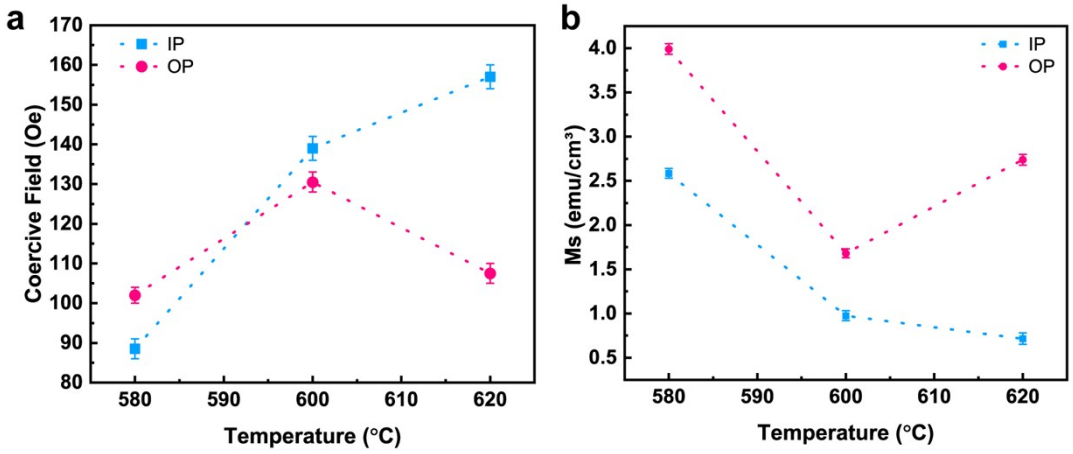

Figure S8. (a) IP and OP coercive field along with (b) saturation magnetization as a function of the growth temperature.

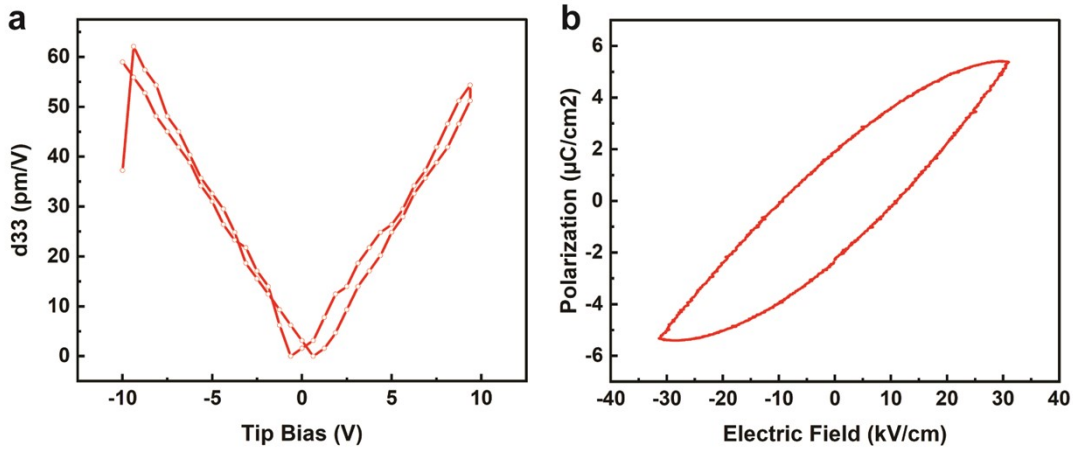

Figure S9. (a) Piezoelectric coefficient d_{33} versus tip bias and (b) polarization hysteresis loop for BAMO-Au thin films grown at 580℃.